Identification and Decomposition of Uranium Oxychloride Phases in Oxygen-Exposed UCl₃ Salt Compositions

Benjamin W. Tuffy,[⊥] Nancy R. Birkner,[⊥] Juliano Schorne-Pinto, Ryan C. Davis, Amir M. Mofrad, Clara M. Dixon, Mina Aziziha, Matthew S. Christian, Timothy J. Lynch, Maxwell T. Bartlett, Theodore M. Besmann, Kyle S. Brinkman, and Wilson K. S. Chiu*

Read Online

ACCESS | Metrics & More | Article Recommendations | Supporting Information

ABSTRACT: Complementary X-ray absorption fine structure (XAFS) spectroscopy and Raman spectroscopy studies were conducted on several UCl_3 concentrations in several chloride salt compositions. The samples were 5% UCl_3 in LiCl (S1), 5% UCl_3 in KCl (S2), 5% UCl_3 in LiCl–KCl eutectic (S3), 5% UCl_3 in LiCl–KCl eutectic (S4), 50% UCl_3 in KCl (S5), and 20% UCl_3 in KCl (S6) molar concentrations. Sample S3 had UCl_3 sourced from Idaho National Laboratory (INL), and all other samples were UCl_3 sourced from TerraPower. The initial compositions were prepared in an inert and oxygen-free atmosphere. XAFS measurements were performed in the atmosphere at a beamline, and Raman spectroscopy was conducted inside a glovebox. Raman spectra were able to confirm initial UCl_3. XAFS and later Raman spectra measured, however, did not correctly match the literature and computational spectra for the prepared UCl_3 salt. Rather, the data shows some complex uranium oxychloride phases at room temperature that transition into uranium oxides upon heating. Oxygen pollution due to failure of the sealing mechanism can result in oxidation of the UCl_3 salts. The oxychlorides present may be both a function of the unknown O_2 exposure concentration, depending on the source of the leak and the salt composition. Evidence of this oxychloride claim and its subsequent decomposition is justified in this work.
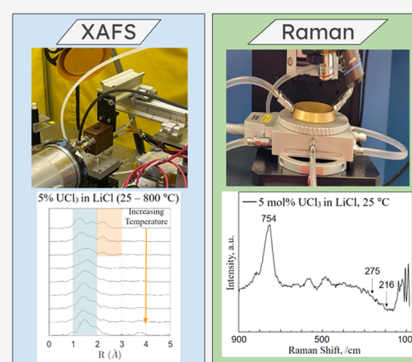
1. INTRODUCTION

The concept of a molten salt reactor had been shown in Oak Ridge National Lab's 1965 Molten Salt Reactor Experiment (MSRE). Recently, the Generation IV International forum recognized the potential of these reactors and the concept of a molten salt reactor (MSR) re-emerged as one of the key models for the development of Gen IV nuclear reactors.[1,2] These Gen IV reactor designs come with a host of benefits, higher operating temperatures, and higher-boiling-point coolant, in the form of molten salt; lead to increased thermodynamic efficiencies; and remove the need for a highly pressurized steam system around the reactor's core. There is also potential to utilize fuels previously classified as spent and achieve a far higher burnup of all nuclear fuels. The concept of molten-state fuel in the form of uranium chlorides brings about further safety benefits in the ability to drain the fuel in the case of a meltdown. As with any new advanced concept there are also new challenges, especially those in the field of nuclear engineering, a comprehensive understanding of the system and all its subsequent components, byproducts, and kinetics is essential to safety and success.

Room-temperature X-ray absorption fine structure (XAFS) scans of the data showed no signs of the intended uranium chloride and a lack of stability between samples as well as during heating. Authors discerned that there was an intense oxygen contamination of the samples and proceeded to rescope goals to identify the occurring phenomena. The U–O–Cl system is composed of a complex phase diagram with several uranium oxides, chlorides, and oxychlorides, possibly dependent on chlorine and oxygen pressures.[3] The chlorides are rather simple, shifting between UCl_3 and UCl_4 dependent on the chlorine concentration, given low enough oxygen content. The uranium oxides are well studied with the U(IV) oxidation state favoring UO_2 at lower oxygen pressures trending up in oxidation states as the oxygen pressure increases, resulting in a U_3O_8 with an average oxidation state (AOS) of 5.33 and eventually in UO_3 with a U(VI) oxidation state.[4−6] The oxychloride region is dominated by a $UOCl_2$ when the oxidation state is U(IV), and while under a higher oxygen presence, UO_2Cl_2 with a U(VI) oxidation state is favored.[7,8] Deeper investigation into the U(VI) oxidation state shows that the number of chlorine atoms bonded seems to be a function of chlorinity of the media and everything from UO_2Cl

Table 1. Sample Compositions Based on Targeted Weights and Actual Compositions Inferred from ICP-OES Analysis

	values in mol %											
salt composition	theoretical			from weighting			from powders − ICP			extracted from Ni liners − ICP		
	LiCl	KCl	UCl$_3$	LiCl	KCl	UCl$_3$	LiCl	KCl	UCl$_3$	LiCl	KCl	UCl$_3$
S1: 5 mol % UCl$_3$ in LiCl	95	0	5	94.76	0	5.24	95.35	0	4.65	95.44	0	4.56
S2: 5 mol % UCl$_3$ in KCl	0	95	5	0	94.93	5.07	0	95.20	4.80	0	95.21	4.79
S4: 5 mol % UCl$_3$ in LiCl-KCl	55.1	39.9	5	56.29	38.78	4.93	60.08	35.23	4.69	-	-	-
S5: 50 mol % UCl$_3$ in KCl	0	50	50	0	50.18	49.82	0	52.19	47.81	0	50.83	49.17
S6: 20 mol % UCl$_3$ in KCl	0	80	20	0	80	20	-	-	-	-	-	-

to UO$_2$Cl$_5$ can be formed with a similar uranyl base.[9−12] Many of these are synthesized and studied within aquo-choro or acidic media. In these cases, it was identified that the typical bonds observed by extended X-ray absorption fine structure (EXAFS) measurements are a shortest-bond-length U-O$_{ax}$ axial bond, signature of the UO$_2$, a medium-bond-length U-O$_{eq}$ binding H$_2$O or OH$^-$ equatorially to the uranium, and some varying number of equatorial longer U−Cl bonds.[12−14]

The original goal of this work was to identify the complex coordinations that occur when UCl$_3$ fuel salt exists in highly ionic LiCl and KCl salt melts, namely, a potential ternary formation. These results would have built on existing UCl$_3$ salt literature and added to the total understanding of these salts.[15−21] Samples were prepared in the absence of O$_2$ and showed near-pure UCl$_3$ after being prepared. However, by the time of data collection in the form of Raman spectroscopy measurements at Clemson University and X-ray absorption spectroscopy (XAS) at SSRL's Beamline 11-2 (SLAC National Accelerator Laboratory, Stanford, CA), almost all data showed oxygen contamination of the system. The intention of the work was subsequently redirected to correctly identifying the phases that occurred as well as the reactions and transitions of the sample due to temperature increase to operationally relevant conditions.

2. EXPERIMENTAL SECTION

2.1. Sample Preparation. Pure uranium trichloride (UCl$_3$) was sourced from TerraPower, and anhydrous lithium chloride (LiCl) and potassium chloride (KCl) were obtained, respectively, from BeanTown Chemicals and VWR with a supplier-reported cation mass fraction purity of >99.9%. UCl$_3$ in lithium chloride (LiCl) potassium chloride (KCl) eutectic without purity specification was sourced from Idaho National Laboratory. The salts were not purified, but their purity has been verified by DSC and XRD, with the results published as Supplementary Material in a previous work.[22] DSC, peak shapes, and structure confirmation through room-temperature X-ray diffraction (XRD) were used to determine melting points to evaluate the purity of the alkali chlorides.[22] The melting points of LiCl and KCl were determined as 879.8 ± 1.4 and 1044.5 ± 1.7 K, respectively, where temperature uncertainties are expanded uncertainties U(T). UCl$_3$ also had a single peak, though broader than those of the alkali chlorides, at 1105.2 ± 4.9 K. Pure UCl$_3$ was also confirmed by Raman spectroscopy.

An MBraun Unilab Pro glovebox under high-purity argon with H$_2$O + O$_2$ concentrations was maintained below 10 ppm, but typically maintained below 5 ppm during regular use. A total mixed mass of at least 100 mg salts was weighted with ±0.1 mg precision on an Ohaus PA84C scale. Samples were then ground in an agate mortar and pestle for 15 min to ensure

homogeneity and then loaded and sealed into custom nickel metal-lined Netzsch 100 μL stainless steel crucibles. These stainless steel crucibles were loaded into a larger crucible and sealed inside the glovebox.

The larger crucible was then removed from the glovebox and loaded into a muffle furnace with a vibration motor-equipped base. Within the muffle furnace, it was heated to 100 K above the expected liquidus temperature and subjected to mechanical agitation for 30 min. This was followed by a rapid quenching in water and subsequent annealing at 723 K for 6 h.

For digested samples, inductively coupled plasma optical emission spectrometry (ICP-OES, PerkinElmer Avio 200) was used to determine the molar ratio of the mixed sample salts. A solution of 5% v/v of HNO$_3$ from the High-Purity Standards (HPS) was dissolved with the Ni liner to avoid any sample loss by a microwave digester (Titan MPS 16 Position, T_{max} = 448.1 K, 20 bars, for 10 min). This was then used as a blank for the ICP-OES as well as a solvent for each sample, and the solutions were diluted to a measurable range. Li, K, and U compositions were calibrated with five different concentrations + blank (0, 1, 2.5, 5, 7.5, and 10 ppm) (Table 1).

2.2. X-ray Absorption Spectroscopy. X-ray absorption spectroscopy (XAS) of S1-S6 was performed at the Stanford Synchrotron Radiation Lightsource (SSRL), Beamline 11-2. Samples were housed in BN crucibles with mechanically sealed screw tops; these crucibles were leak-tested by inversion of the molten sample. During the experiment, the sample sits within a copper heating jacket consisting of a ceramic heating element and channels for water chiller cooling. Temperature calibration is done by applying a voltage across the heating element and recording voltage at desired temperatures using a K-type thermocouple. A fourth-order polynomial is used to calibrate a complete temperature curve relating the voltage to temperature. This heater and experimental design were shown to be successful in preliminary in situ X-ray studies of Zr and Sr salts.[23,24] The U L3 absorption edge at 17,166 eV was interrogated using monochromatic X-rays. Energy wavelengths of 240 eV below the edge to 800 eV above the absorption edge were used to generate X-ray absorption fine structure (XAFS) spectra. Transmission data is recorded by measuring the change in intensity of the beam in ion chambers before and after the sample. An yttrium foil is placed between the second and third ion chambers, after the sample, and is used as a reference to calibrate the E_0 while preserving data related to the signature of the U L3-edge. The XAS spectra were recorded in transmission mode at room temperature, at select temperatures up to 800 °C, as well as again at 25 °C after the sample resolidified following the cool-down procedure. At each temperature step, the heater temperature was allowed to equilibrate for 30−40 min. Athena[25] was used to process, calibrate, and otherwise clean up the energy space data. While
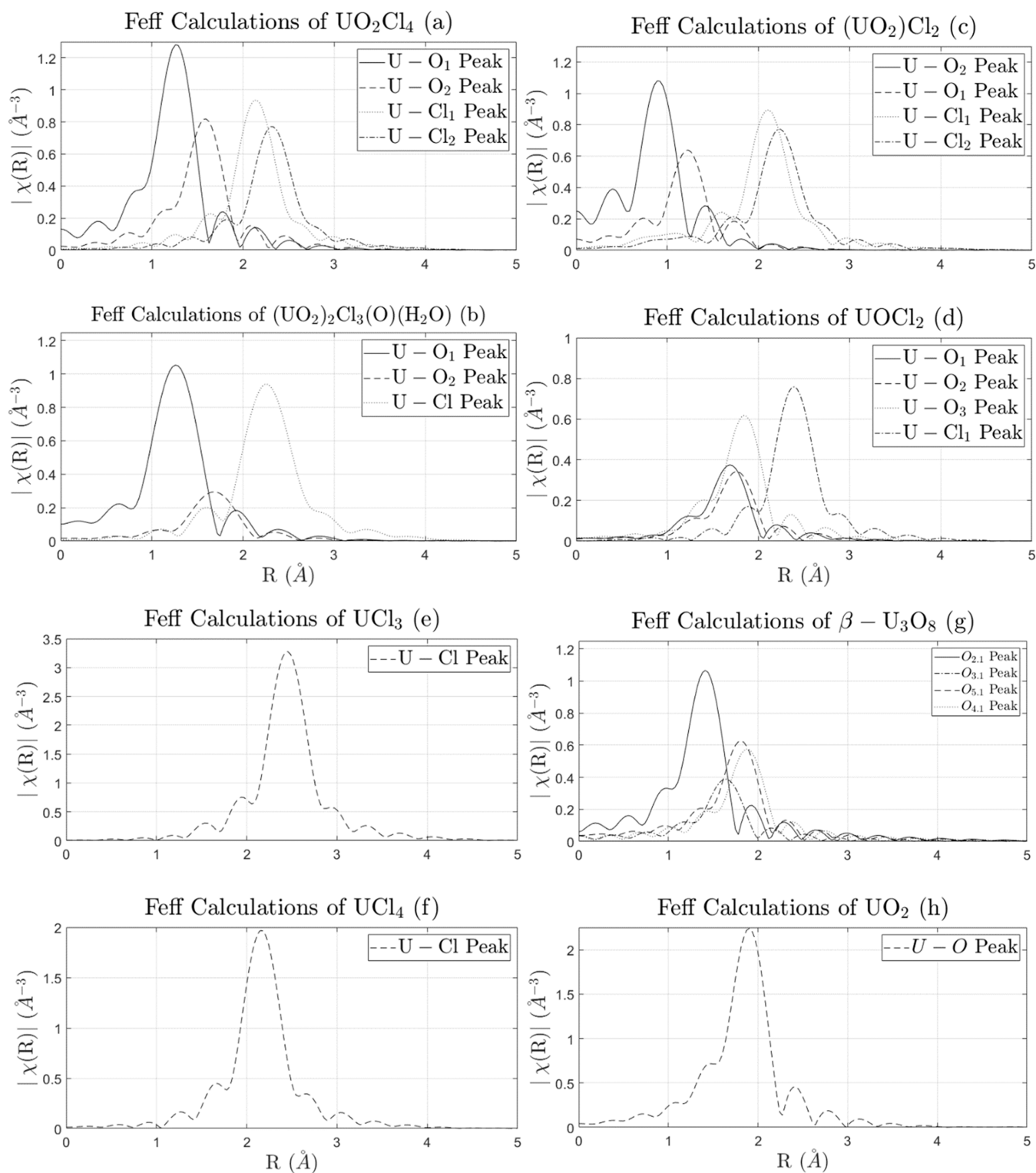
Figure 1. FEFF calculation of several uranium oxychlorides (a−d), uranium chlorides (e, f), and uranium oxides (g, h).[9,10,28−32]

X-ray data was taken and heating occurred, the BN sample holders were exposed to atmosphere and sealed only with a mechanical BN screw top. Time of first exposure to the atmosphere was not recorded; thus, the exactness of the kinetics is left as an open-ended question.

For Sample 5, the same energy range of 240 eV below to 800 eV above the L3-edge is used, but the data is instead collected at room temperature only in fluorescence mode to a 100

element XRF detector located perpendicular to the beam. Absorption mode was not possible for S5 due to the high concentration of uranium resulting in high beam attenuation.

2.3. Raman Spectroscopy. Prior to each experiment, an aliquot of sample was loaded into a specially made BN crucible (7 mm OD, 6 mm ID, 3 mm deep; Stanford Advanced Materials) within a glovebox controlled for oxygen and water atmosphere (<1 ppm O_2 and H_2O). To safeguard against
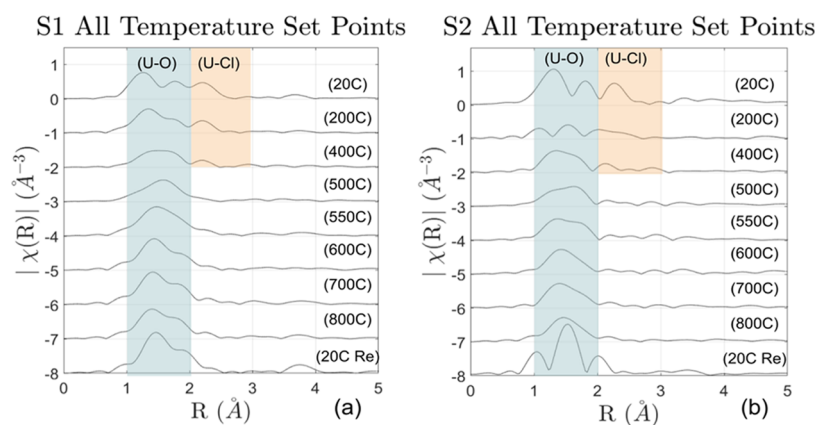
Figure 2. XAS scans at all temperature set points for (a) S1 5% UCl$_3$ in LiCl and (b) S2 5% UCl$_3$ in KCl. U−Cl and U−O bond lengths highlighted.

cross-contamination, a new crucible was used for each experiment. The sample-loaded crucible was mounted into an *in situ* Linkam TS1500 high-temperature stage. The stage was sealed at all ports, making use of one of its designed features, to minimize atmospheric exposure during either transport or measurement. To further diminish the likelihood of sample exposure, the in situ assemblage was placed into a gasket-sealed container before removal from the glovebox and then taken immediately to the Raman suite where it was then associated with the instrument under continuous argon flow (55 cc/min). Total time for transport and association was within 1/2 h.

Raman scattering spectroscopy was done with the Horiba LabRAM Evolution Raman microscope equipped with an 800 mm focal length spectrograph, a cooled back-illuminated deep-depleted 1024 × 256 pixels CCD detector using a 100 mW 532 nm laser with no attenuation, and interchangeable magnification objectives. The confocal hole aperture was set to *approx.* 200 μm and the grating to 1800/mm. Using the Raman microscope, samples were aligned using the laser beam, which was focused with a 100× achromatic microscope objective lens. Each spectrum was corrected by the pre-recorded instrument-specific response to a calibrated white light source, namely, the intensity correction system. Horiba Scientific's LabSpec 6 Spectroscopy Suite, supplied with the Raman, was used in this work.

Raman spectra over the range of 900−90/cm contain vibrational fingerprint regions for uranium oxides and uranyl chlorides, which contribute to the refinement of their identification. As such, spectra of the measured samples were plotted to focus on the regions of interest. For all samples, *in situ* Raman spectroscopy was applied from room to molten temperature while nonpolarized spectra were recorded. A minimum of two aliquots of sample were measured, if their spectra matched. Although each spectrum was collected within seconds, because of the careful application of our developed techniques for measurement of molten salts from room to molten temperatures, Raman experiments were time-intensive.[26] The molten salts have a vapor pressure that allows sublimation at molten temperatures. As in our previous work, only a small portion of the molten salt sample sublimated and subsequently condensed into a faint thin film of salt on the quartz viewing window. Measurements of sublimated molten salts that comprise this thin veneer have yet to be anything other than identical to that of the bulk sample vibrational

frequencies, although at a lower intensity. Measurements were done with quicker acquisition time at the melting point temperature and performed after all lower-temperature spectra had been collected.

3. COMPUTATIONAL APPROACH

The XAS measurements did not successfully align nor fit with any expected uranium chloride structures. Subsequently, a thorough literature examination and comparison of the data was completed to try and identify and make sense of the extended X-ray absorption fine structure (EXAFS) results. Selections of the compounds were made primarily from the U−O−Cl phase diagrams.[3,7] Additionally, the uranyl compounds formed from the UO$_2^{2+}$ ion in high-chlorine concentration solutions show similar X-ray spectra to the room temperature data[12] as well as several uranium oxides.[27] FEFF calculations were performed using Artemis to generate R-space from selected CIF files.[25] Theoretical spectra of the most common oxides and oxychlorides, as well as the expected uranium chlorides are shown in Figure 1. These spectra show peaks at locations in R-space corresponding to interatomic bond distance found in each structure. A superposition of several peaks would be required to represent any of the data seen in the low-temperature XAFS spectra. Through this data, the immediate distinction is that every U−Cl bond length peak occurs above 2 Å while every U−O bond signature appears below the 2 Å demarcation.

4. RESULTS AND DISCUSSION

4.1. X-ray Absorption Spectroscopy. A cursory look at the samples' EXAFS scans in R-space at 20 °C, Figure 3, shows a messy scattering of interatomic distances between the uranium atoms and its nearest neighbors. This lack of consistency is likely due to multiple phases existing; this variance will be attributed to the ongoing kinetics of oxygen exposure as well as salt composition of the samples. A full view of all temperature set points for all samples is given in Figure 2. There does seem to be a correlation in the trends of the data, that is, in almost all samples, some 3 bond lengths are present at 20 °C. This suggests that prior to heating, the samples were composed of some uranium oxychlorides potentially in combination with some pure uranium oxides or chlorides. Interpretations of the EXAFS region of the data show that as the samples were heated, the longest bond, affiliated with U−

Table 2. XANES White Line Peaks (Absorption Edge Energy) for All Temperature Set Points for S1−S6

temperature (°C)	S1: 5 mol % UCl$_3$ in LiCl	S2: 5 mol % UCl$_3$ in KCl	S3: 5 mol % UCl$_3$ in LiCl-KCl	S4: 5 mol % UCl$_3$ in LiCl-KCl	S6: 20 mol % UCl$_3$ in KCl
20	17168.3	17165.9	17168.7	17168.1	17166.3
200	17168.6	17166.4	17168.9	17168.5	17167.5
370	-	-	17169.1	17168.8	-
400	17169.1	17168.9	17169.1	17169.1	17169.2
500	17169.5	17169.3	17169.4	17169.2	17169.2
550	17169.5	17169.2	-	-	17169.2
600	17169.5	17169.5	-	17169.4	17169.3
700	17169.5	17169.4	-	17169.4	17169.5
800	17169.4	17169.4	-	17169.4	17169.5
resolidified	17169.5	17169.5	17169.4	17169.6	17169.6
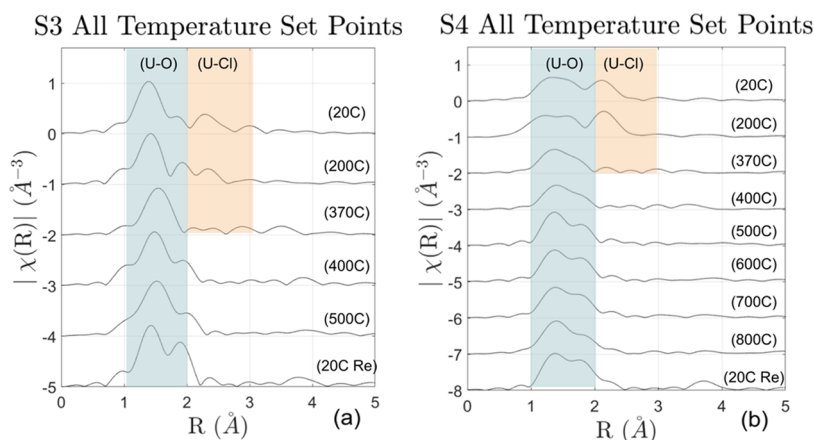
Figure 3. XAS scans at all temperature set points for (a) S3 5% UCl$_3$ (INL) in LiCl−KCl eutectic and (b) S4 5% UCl$_3$ (TerraPower) in LiCl−KCl eutectic. U−Cl and U−O bond lengths highlighted.
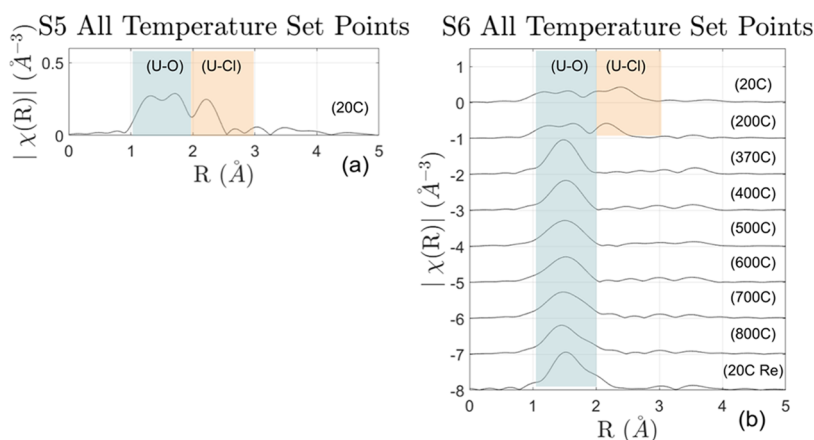
Figure 4. XAS scans at all temperature set points for (a) S5 50% UCl$_3$ in KCl and (b) S6 20% UCl$_3$ in KCl. U−Cl and U−O bond lengths highlighted.

Cl in the case of these compounds, vanishes and a common peak shape emerges between 1 and 2 Å at high temperatures.

The hypothesis that the structure of the uranium in the samples is some non-unanimous oxychloride in low-temperature scans while converging to a similar, stable, uranium oxide as the sample is heated and is supported by the X-ray absorption near-edge structure (XANES) spectra as well. Table 2 reports white line peaks of the XANES region of the spectra; this white line peak is correlated to the U L3 absorption edge. Sample S5 does not have XANES data presented due to only one temperature scan being taken, the shift in edge energy is the relevant information. This edge energy is a function of average oxidation state (AOS) of the uranium atoms being irradiated by incident X-rays. Table 2 then indicates an inconsistent AOS at low temperatures with the L3-edge ranging between 17,165.9 and 17,168.7 eV, which indicates a variance in the oxidation state of at least 1−2 eV in these preheated samples.[20,21] Samples S2 and S6 show the lowest white line edge energy and the largest shift as the samples heat; this indicates that they have a lower AOS of the uranium at room temperature than S1, S3, and S4. At 700 and 800 °C, the edge energies were unanimously 17169.4 or 17169.5 eV. This constant AOS is likely consistent with a similar compound forming between all samples.
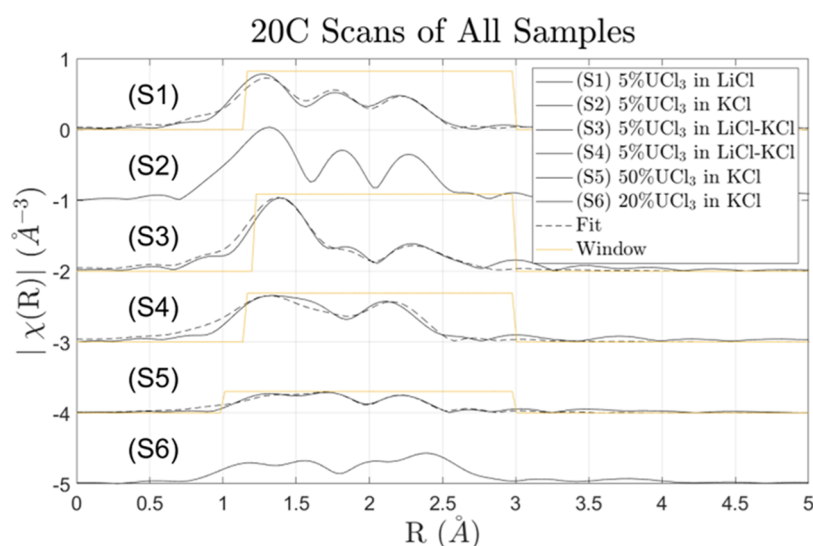
Figure 5. R-space of S1−S6 at 20 °C, accomplished fits for S1, S3, S4, and S5 shown as dashed lines.

Table 3. EXAFS Fitting Parameters for R-Space Fits Shown in Figure 3 (S1, S3, S4, S5)

20 °C UO_xCl_y fitting parameters										
sample	S_0^2	E_0	R_1(Å) U-O_1	R_2(Å) U-O_2	R_3(Å) U−Cl	σ^2 $(10^{-3}$ Å$^2)$	N_1	N_2	N_3	R factor
S1 (a)	0.90	−3.1	1.75 ± 0.02	2.21 ± 0.15	2.64 ± 0.01	5.7 ± 2.0	2.0	4.4	4.6	0.010
S3 (c)	0.90	10	1.79 ± 0.03	2.34 ± 0.13	2.83 ± 0.02	4.4 ± 2.9	2.4	1.4	1.5	0.044
S4 (d)	0.90	−3.1	1.75 ± 0.02	2.21 ± 0.00	2.64 ± 0.17	10.6 ± 1.1	2.0	4.3	4.4	0.010
S5 (e)	0.60	2.7	1.73 ± 0.03	2.26 ± 0.05	2.67 ± 0.14	5.4 ± 1.5	0.7	2.4	1.7	0.193

This phenomenon is thought to be the decomposition of a variety of oxychloride structures under heating. It is already known that these oxychloride structures decompose around 500 °C.[3,8] The objective is to show that these spectra reflect oxychloride decomposition. The FEFF calculations shown in Figure 1 are a clear separation above and below 2 Å, graphically corresponding to U−Cl and U−O bonds, respectively. These regions are highlighted and labeled in the spectra of Figures 2−4. This analysis then proposes that at the first 2−3 temperature set points, depending on the sample, there exist multiple U−O and U−Cl bonds before heating. The peaks correlated to the U−Cl region clearly vanish by 500 °C and above, implying that no uranium chlorides or oxychlorides exist, leaving only some uranium oxide. Complete oxidation, which seems to occur at higher temperatures, will result in only UO_2^{2+} or U_3O_8 phases remaining. Fits and justification of this U_3O_8 claim using the same spectra are presented in an additional manuscript.[33] FEFF calculations and fitting were only completed for the first coordination shell, excluding any U−U bonds that the CIF files indicate. This is due to the increase in complexity of fitting as well as lack of resolution beyond the 4 Å range where this occurs. However, it is worth noting that between the highest-temperature scans and the resolidified scans in Figures 2−4, features around 4 Å may indicate solidification through the formation of new U−U bonds.

To properly justify that these spectra reflect oxychlorides, several EXAFS fits were attempted. The CIF files used to generate the fits were UO_2Cl_4 and $(UO_2)_3Cl_3(O)(H_2O)$ oxychlorides, both with a U(VI) oxidation state.[10,34] Fits were only achieved for S1, S3, S4, and S5, at 20 °C and are shown in Figure 5. Corresponding EXAFS parameters are reported in Table 3. This U(VI) oxidation state is favored simply because

the oxychlorides corresponding to the U(III) and U(IV) oxidation states were not able to generate accurate fits with reasonable guess parameters. This would imply that we are studying some uranyl (UO_2^{2+}) base with additional oxygen and chlorine equatorial bonds. Recall that S2 and S6, which were not able to generate a fit at room temperature, showed the lowest absorption edge energy and lowest AOS in Table 2. This would suggest that S2 and S6 are more likely a U(IV) oxidation state that was not able to be fitted to any structure file.

Though it is likely impossible to make a perfect fit given the chemical and phase transience, the fits are meant to show that the signature bond lengths of these oxychloride compounds were seen. The radial distances accurately reflect the expected values for an oxychloride with 2 U−O bond lengths and 1 U−Cl bond length. Each bond is given a corresponding coordination number guess. Functionally, this allows the number of oxygens and chlorines bonded to be flexible, i.e., stronger peaks indicate uranium bonded with more of that specific atom at that bond length. Samples with higher N_3 coordination number reflect a higher chlorine-to-uranium coordination. Note that a mixing parameter and coordination number both scale with the same amplitude factor, S_0^2, so they are treated as one parameter due to the limitations of this work. The reality that these were likely multiple-phase compounds means these coordination numbers may also reflect the ratio of uranium oxychlorides to uranium oxides as well as the chlorine coordination of the oxychlorides.

4.2. Raman Spectroscopy. Note that initially Raman spectra were able to confirm the prepared UCl_3; these phenomena occur after some duration of testing. Considering the two apical uranyl oxygens as poles, the uranyl complex could have 2−6 equatorial ligands. The bare uranyl ion, which

Table 4. Sample S1. Raman Vibrational Frequencies and Band Assignments Relevant to the U−O−Cl Moiety in 5 mol % UCl$_3$ in LiCl Exposed to Oxygen

S1, T °C	U AOS	$\nu_8(E_g,\ UO_2Cl_2)$ approx. 208−220	$\nu_2(A_{1g},\ U-Cl_4)$ approx. 265−275	high region, 1/cm $\nu_1(A_{1g}$ U-O, $UO_2^{(2+)}$ of γ-UO$_3$)
S1, 25 °C	U(5.33−6)	216	275	754
S1, 400 °C	U(5.33−6)	208	271	748
S1, 550 °C	U(5.33−6)	214	270	748
S1, 600 °C[a]	U(5.33)	219	269	704

[a]Notation: Temperature of the melt.

Table 5. Sample S2. Raman Vibrational Frequencies and Band Assignments Relevant to the U−O−Cl Moiety in 5 mol % UCl$_3$ in KCl Exposed to Oxygen

S2, T °C	U AOS	$\nu_8(E_g,\ UO_2Cl_2)$ approx. 208−220	$\nu_2(A_{1g},\ U-Cl_4)$ approx. 265−275	high region, 1/cm $\nu_1(A_{1g}$ U-O, $UO_2^{(2+)}$ of γ-UO$_3$) and ν(O-U-O, β-U$_3$O$_8$)
S2, 25 °C	U(5.33−6)	215	267	(742ν_1 + ν779s)db
S2, 400 °C	U(5.33−6)	212	273	(771ν_1 + ν739s)db
S2, 550 °C	U(5.33−6)	213	271	770ν_1
S2, 600 °C	U(5.33−6)	216	270	770ν_1
S2, 800 °C[a]	U(5.33)	218	270	ν667m

[a]Notation: Temperature of the melt; strong is s; medium is m; doublet is db.

Table 6. Sample S4. Raman Vibrational Frequencies and Band Assignments Relevant to the U−O−Cl Moiety in 5 mol % UCl$_3$ in Eutectic Li−K−Cl Exposed to Oxygen

S4, T °C	U AOS	$\nu_8(E_g,\ UO_2Cl_2)$ approx. 208−220	$\nu_2(A_{1g},\ U-Cl_4)$ approx. 265−275	high region, 1/cm ν(O-U-O, β-U$_3$O$_8$) commonly, 753; 798; 809; 810
S4, 25 °C	U(5.33−6)	210	273	670; 637vw
S4, 370 °C	U(5.33−6)	206	270	634vw
S4, 400 °C	U(5.33−6)	204	271	682; 665vw
S4, 500 °C[a]	U(5.33−6)	212	271	633; 641w
S4, 800 °C	U(5.33)	215	273	798w; 633vw

[a]Notation: Temperature of the melt; weak is w; very weak is vw.

has a linear symmetry, most certainly will not remain an isolated ion, particularly in a molten salt environment. As previously illustrated and discussed by Jones (1958),[35] all molecular symmetries of any uranyl complex will have two symmetric stretching vibrational frequency modes. These are the ν_1 and ν_2, which correspond with the U−O and U−Ligand symmetric stretching bonds. If the ν_2 ligands are halides, then the U−O bonds will be stronger bonds. However, the U−Cl bonds influence the U−O bond strength and as such the two vibrational modes should always be evaluated together before assuming that it is justifiable to neglect the ν_2 effect. The vibrational frequencies of ν_1 and ν_2 corresponding to U=O and U−Cl are indicators of how closely the O− or Cl− ligands are held to the central U atom in the uranyl complex and the strength of the U=O and U−Cl bonds. Uranyl ν_1 band shift, or lack thereof, thus may be used to identify the level of Cl saturation although the ν_1 relates directly to the U−O bond. For example, a blue shift occurs for ν_1 with temperature increase for the lesser Cl-substituted uranyl complexes such as $UO_2Cl^{(+)}$, $UO_2Cl_2^{(0)}$, and $UO_2Cl_3^{(1-)}$. Dargent and colleagues[36] observed that blue shifts in bands occurred for the lesser Cl-substituted uranyl complexes by as much as +3/cm over the temperature range 25−350 °C. Conversely, the ν_1 is insensitive to temperature for the more highly Cl-saturated uranyl complexes, $UO_2Cl_4^{(2-)}$ and $UO_2Cl_5^{(1-)}$. If the ν_1 does not shift with increased temperature, then the uranyl moiety is more highly Cl-saturated while simultaneously indicating that the U=O bond strength is unchanged. The increase or decrease in Cl saturation about the equatorial plane changes the corresponding vibrational frequency of the fully symmetric

ν_2. The effect on ν_2 informs about the length and strength of the U−Cl bonds, since ν_2 tracks positively with U−Cl bond strength.

Halides have a pronounced influence as ligands on the ligand-$UO_2^{(2+)}$ moiety. As a halide ligand orbital overlaps with a uranium atom nonbonding orbital, the electron density of the U−Cl shifts significantly thereby increasing the charge over the uranium atom. The U=O bond length may increase due to the charge density shift promoting greater oxygen atom repulsion. Thus, as they are based on the nearness to which the central uranium atom holds ligands, the force constants of U=O and U−Cl and the "felt" masses of $O^{(2-)}$ and $Cl^{(-)}$ ligands change due to the halide saturation level. Band shifts of the ν_1 due to the effects of alkali cations Li, Na, K, and Cs on uranyl complexes were the focus of Polovov (2008).[37] Dargent (2014)[36] studied the U−O symmetric stretching mode $\nu_1(A_{1g}$ U-O, $UO_2^{(2+)})$ changes in various concentrations of chlorinity from 25 to 350 °C, exploring more deeply the linear relation between the ν_1 and the number of Cl ligands in various levels of Cl-substituted uranyl U−O−Cl moieties previously identified by Nguyen-Trung.[38] Fujii[39] additionally focused on the polarization effects of Li, Na, K, and Cs alkali cations on the mechanism of interaction of Cl and oxygen with the $UO_2Cl_4^{(2-)}$ uranyl complex by examining the changes that resulted in the $\nu_1(A_{1g}$ U-O, $UO_2^{(2+)})$, $\nu_2(A_{1g}$ U-Cl$_4$), and $\nu_8(E_g,\ UO_2Cl_2)$. The vibrational frequency $\nu_8(E_g,\ UO_2Cl_2)$ correlates with U−O−Cl uranyl $UO_2Cl_4^{(2-)}$ complex stability.[39] Applying ν_1, ν_2, and ν_8 is a sensitive analytical tool for the more highly Cl-saturated uranyl complex.

Table 7. Sample S5. Raman Vibrational Frequencies and Band Assignments Relevant to the U−O−Cl Moiety in 50 mol % UCl$_3$ in KCl Exposed to Oxygen

S5, T °C	U AOS	$\nu_8(E_g,\ UO_2Cl_2)$ approx. 208−220	$\nu_2(A_{1g},\ U-Cl_4)$ approx. 265−275	ν(O-U-O, β-U$_3$O$_8$) commonly, 753; 798; 809; or 810
S5, 25 °C	U(5.33)	211	272	809m; 798m
S5, 400 °C	U(5.33)	211	272	809m; 797m
S5, 550 °C^a	U(5.33)	211	273	809m; 798m
S5, 600 °C	U(5.33)	211	272	809m; 798m
S5, 800 °C	U(5.33)	211	272	809m; 797m

^{a}Notation: Temperature of the melt; medium is m.

Similar to the UO$_2$Cl$_4$$^{(2−)}$ uranyl complex of D$_{4h}$ symmetry studied by Fujii and colleagues,[39] analyses of the Raman spectra of the current work indicated that the more highly Cl-saturated complex UO$_2$Cl$_4$$^{(2−)}$ is present in all samples. Although they may not be purely UO$_2$Cl$_4$$^{(2−)}$, the logic still holds in the current work as the samples track consistently. Applying the ν_1, ν_2, and ν_8 vibrational modes to the current work can delineate the relative stability of the U−O−Cl uranyl complexes, the level of Cl saturation, the effect of the chemical environment on lengthening or decreasing the U═O and U−Cl chemical bonds, and the temperature at which the most stable phase evolved. This suggests that the samples retain chloride as ligands into the melt until the final stable phase is formed. Further, it is reasonable to hypothesize that kinetics gated the transformation to the final β-U$_3$O$_8$ stable phase at molten temperatures. Raman vibrational frequencies (ν_1, ν_2, and ν_8) as a function of temperature were examined to locate trends in samples S1, S2, S4, S5, and S6 corresponding to the uranyl U−O−Cl complex characteristics and stability. The results are summarized in Tables 4−8 and in the SI Figures.

Table 8. Sample S6. Raman Vibrational Bands and Assignments Relevant to the U−O−Cl Moiety in 20 mol % UCl$_3$ in KCl Exposed to Oxygen

S6, T °C	U AOS	$\nu_8(E_g,\ UO_2Cl_2)$ approx. 208−220	$\nu_2(A_{1g},\ U-Cl_4)$ approx. 265−275	$\nu_1(A_{1g}\ U-O,\ UO_2^{(2+)},\ \gamma$-UO$_3$) and ν(O-U-O, β-U$_3O_8$)
S6, 25 °C	U(5.33−6)	215	278	(804ν_1 + ν796)db
S6, 400 °C	U(5.33−6)	205	274	803ν_1
S6, 550 °C	U(5.33−6)	209	272	795ν_1
S6, 600 °C^a	U(5.33)	217	277	794ν_1
S6, 800 °C	U(5.33)	218	274	793ν_1

^{a}Notation: Temperature of the melt; doublet is db.

4.2.1. 5 mol % UCl$_3$ in LiCl (Sample S1). For S1, two different stabilities occur for the $\nu_8(E_g,\ UO_2Cl_2)$ at 25 °C demonstrating the presence of the two U−O−Cl moieties for the structures with the AOS of U(5.33) and U(6). The U−O−Cl complexes in the sample were destabilized at 400 °C. With a further increase in temperature, the stability increases until the final β-U$_3$O$_8$ is formed. As reported elsewhere,[33] the final stable phase at molten temperature is β-U$_3$O$_8$ for S1 with a corresponding reduction in initial AOS of U(5.33−6) at 25 °C to U(5.33) in the melt. Here, we find that the greatest $\nu_8(E_g,\ UO_2Cl_2)$ for S1 is at the molten temperature indicating that indeed the most stable complex was formed in the melt. With the formation of β-U$_3$O$_8$ as the final stable phase at molten temperature, the U−Cl vibrational frequency mode $\nu_2(A_{1g},\ U-Cl_4)$ in S1 decreases relative to those at lower temperatures, correlating with diminished U−Cl chemical bond strength. The U−Cl bond length would not necessarily be changing as a

function of bond strength, and further evidence would be needed to determine this. The $\nu_1(A_{1g}\ U-O,\ UO_2^{(2+)})$ vibrational frequency demonstrates temperature dependence with a 50/cm difference between the ν_1 at room and molten temperatures. Additionally, it indicates diminished strength in the U═O chemical bond from room to molten temperature. The shift in ν_1 is very small and occurs from 25 to 400 °C, suggesting that the Cl saturation of the complex puts it somewhere between UO$_2$Cl$^{(+)}$, UO$_2$Cl$_2$$^{(0)}$, and UO$_2Cl_3$$^{(1−)}$. However, this is not a blue shift, which indicates that the U AOS is not remaining constant but is instead decreasing. Interestingly, between 400 and 550 °C, the ν_1 does not shift, which suggests that the Cl ligand substitution level has increased to UO$_2$Cl$_4$$^{(2−)}$ or UO$_2$Cl$_5$$^{(1−)}$ as these U−O−Cl moieties are insensitive to temperature and do not shift the ν_1 band position. Finally, with an increase to the melt temperature, the ν_1 significantly red shifts to a lower vibrational frequency by 48/cm, indicating reduction of the U AOS to that of the β-U$_3$O$_8$ with a simultaneous decrease in U═O bond strength.

4.2.2. 5 mol % UCl$_3$ in KCl (Sample S2). At 25 °C, S2 has a very broad and prominent ν(β-U$_3$O$_8$) band in addition to that of the uranyl $\nu_1(A_{1g}\ U-O,\ UO_2^{(2+)},\ \gamma$-UO$_3$), which is the cause of the split or doublet band in the high-frequency region of the spectrum. The uranyl ν_1 band blue-shifts from 742 to 771/cm with a temperature increase from 25 to 400 °C, indicating U═O chemical bond strength increase for the ν_1 molecular symmetry U−O−Cl complex. Meanwhile, the ν(β-U$_3$O$_8$) redshifts from 779 to 739/cm correlated with weakening of U═O bond strength. Here too, from 25 to 400 °C, the Cl substitution level must be increasing to that of either the UO$_2$Cl$_4$$^{(2−)}$ or the UO$_2$Cl$_5$$^{(1−)}$ species as subsequent temperature increases do not shift the ν_1 or the ν(β-U$_3$O$_8$) further reaching the melt. Correspondingly, the vibrational frequency of the $\nu_2(A_{1g},\ U-Cl_4)$ mode increases from room temperature to 400 °C with a corresponding decrease in complex stability. The ν_2 then decreases as temperature is increased from 400 to 550 °C with the change in stability increasing slightly. Subsequently, the U−Cl bond strength remains unchanged from 550 °C into the melt although stability continues to increase as the final stable phase β-U$_3$O$_8$ is produced.

4.2.3. 5 mol % UCl$_3$ in Li−K−Cl (Sample S4). For S4, stability is greatest in the melt and weakest at 400 °C as it is for the previous samples. Starting out fairly stable, S4 then gradually decreases in stability from 25 to 400 °C and then subsequently increases until forming the fully stable final phase in the melt. The U−Cl chemical bond strength decreases from 25 to 400 °C, then remains fairly constant (±1/cm) up into the melt at 500 °C, and then increases slightly at 800 °C. The ν(O-U-O, β-U$_3$O$_8$) mid-region multiplex of bands range in their intensity from very weak to weak at all temperatures. Were it not for the application of the vibrational frequencies

(ν_8 and ν_2), the changes in the sample occurring as a function of temperature might have been overlooked.

4.2.4. 50 mol % UCl$_3$ in KCl (Sample S5). The stability of S5, as indicated by the ν_8(E$_g$, UO$_2$Cl$_2$), is unchanging over the molten temperature range of 25 to the 800 °C. The U=Cl and U=O bond strengths do change slightly over the measured temperatures but within the measurement error (± 1/cm). Thus, it appears that the U−O−Cl complex in S5 begins and ends as the most stable phase also occurs in the melt of the previous samples. The Cl substitution level of the U−O−Cl complex may likely be that of either the UO$_2$Cl$_4^{(2-)}$ or the UO$_2$Cl$_5^{(1-)}$ due to insensitivity to temperature increase.

4.2.5. 20 mol % UCl$_3$ in KCl (Sample S6). At room temperature, S6 has a very prominent ν(O-U-O, β-U$_3$O$_8$) vibrational frequency that is second only to that of the uranyl ν_1(A$_{1g}$ U−O, UO$_2^{(2+)}$, γ-UO$_3$), which accounts for the split or doublet band in the high-frequency region of the spectrum. The uranyl ν_1 does not shift with temperature increase from 25 to 400 °C within the measurement error (± 1 /cm), indicating no change in U=O chemical bond strength for the ν_1 molecular symmetry U−O−Cl complex. The ν(O-U-O, β-U$_3$O$_8$), in contrast, disappears at 400 °C. Insensitive to the temperature change, from 25 to 400 °C, the Cl substitution level in the uranyl complex may be similar to either UO$_2$Cl$_4^{(2-)}$ or UO$_2$Cl$_5^{(1-)}$. The stability of the complex decreases at 400 °C as does the U−Cl chemical bond strength, which would allow for elongation of these bonds. The stability of the complex then increases with an increase in temperature to 550 °C. Here, the ν_1 vibrational frequency decrease from 803/cm to 795/cm is correlated with a decrease in U=O bond strength. Subsequently, the U−Cl bond strength diminishes slightly as well. The ν_1 vibrational frequency red-shifts very slightly (1/cm) as the temperature is increased through 550 °C (795/cm), 600 °C (794 /cm), and 800 °C (793/cm), which suggests a high Cl substitution level (e.g., UO$_2$Cl$_4^{(2-)}$ or UO$_2$Cl$_5^{(1-)}$) in addition to an unchanged U=O chemical bond strength and increased complex stability consistent with increasing ν_8. Additionally, the stability of the melt at 600 °C is similar to that at 800 °C (± 1/cm) molten temperature, indicating that the final stable phase β-U$_3$O$_8$ was formed at the melting point. The U−Cl strength increases at 600 °C in the melt but subsequently decreases again with temperature increase to 800 °C perhaps inciting full conversion of the sample to β-U$_3$O$_8$.

5. CONCLUSIONS

Complementary X-ray absorption fine structure (XAFS) spectroscopy and Raman spectroscopy were applied to several concentrations of UCl$_3$ in molten K- and Li-chloride salts. The XAFS results suggest that U−O−Cl complexes were present, with uranium chlorides transforming into a complex uranium oxychloride before further transformation to β-U$_3$O$_8$. The XAFS results correlate well with those of the Raman spectroscopy studies. The more highly Cl-saturated complex UO$_2$Cl$_4^{(2-)}$ was found to be present in all samples. Vibrational frequencies ν_1, ν_2, and ν_8 were used to characterize the U−O and U−Cl bond strength changes as well as the stability of the uranyl complexes. In the melt, much of the U−O−Cl complexes demonstrated the formation of β-U$_3$O$_8$. The presence of the UO$_2$Cl$_4^{(2-)}$ in the highly saturated Cl samples, the temperatures at which stable state was reached, and the duration that the chlorine ligands remained in the melt, reasonably suggest that the process of reaching the stable β-

U$_3$O$_8$ phase is gated by kinetics. Exposure to atmospheric oxygen was clearly very small, and correctly understanding these structures, their formation, and their stability in oxygen-exposed fuel salts is essential for molten salt research and applications.

■ ASSOCIATED CONTENT

Ⓢ Supporting Information

The Supporting Information is available free of charge at https://pubs.acs.org/doi/10.1021/acs.jpcb.2c09050.

> A schematic of the XAFS spectroscopy beamline setup and sealing mechanism is shown in Figure SI-1. The setup and sealing mechanism for the Linkam TS1500 high-temperature stage for Raman spectroscopy are shown in Figures SI-2 and SI-3. The Raman spectra and table of vibrational frequencies and band assignments for Samples S1, S2, S4, S5, and S6 are shown in Figures SI-4 to SI-8 (PDF).

■ AUTHOR INFORMATION

Corresponding Author

Wilson K. S. Chiu − *Department of Mechanical Engineering, University of Connecticut, Storrs, Connecticut 06369-3139, United States;* ⓘ orcid.org/0000-0001-7402-4951; Email: wchiu@engr.uconn.edu

Authors

Benjamin W. Tuffy − *Department of Mechanical Engineering, University of Connecticut, Storrs, Connecticut 06369-3139, United States*

Nancy R. Birkner − *Department of Materials Science and Engineering, Clemson University, Clemson, South Carolina 29634-0901, United States*

Juliano Schorne-Pinto − *Nuclear Engineering Program, University of South Carolina, Columbia, South Carolina 29208, United States;* ⓘ orcid.org/0000-0003-4208-4815

Ryan C. Davis − *Stanford Synchrotron Radiation Lightsource, SLAC National Accelerator Laboratory, Menlo Park, California 94025, United States*

Amir M. Mofrad − *Nuclear Engineering Program, University of South Carolina, Columbia, South Carolina 29208, United States*

Clara M. Dixon − *Nuclear Engineering Program, University of South Carolina, Columbia, South Carolina 29208, United States*

Mina Aziziha − *Nuclear Engineering Program, University of South Carolina, Columbia, South Carolina 29208, United States;* ⓘ orcid.org/0000-0003-4001-6413

Matthew S. Christian − *Nuclear Engineering Program, University of South Carolina, Columbia, South Carolina 29208, United States;* ⓘ orcid.org/0000-0002-3416-413X

Timothy J. Lynch − *Department of Mechanical Engineering, University of Connecticut, Storrs, Connecticut 06369-3139, United States*

Maxwell T. Bartlett − *Department of Mechanical Engineering, University of Connecticut, Storrs, Connecticut 06369-3139, United States*

Theodore M. Besmann − *Nuclear Engineering Program, University of South Carolina, Columbia, South Carolina 29208, United States*

Kyle S. Brinkman − *Department of Materials Science and Engineering, Clemson University, Clemson, South Carolina*

29634-0901, United States; ● orcid.org/0000-0002-2219-1253

Complete contact information is available at:
https://pubs.acs.org/10.1021/acs.jpcb.2c09050

Author Contributions

⊥B.W.T. and N.R.B. are Co-first authors.

Notes

The authors declare no competing financial interest.

■ REFERENCES

(1) Williams, D. F.; Britt, P. F. *Technology and Applied R&D Needs for Molten Salt Chemistry: Report for the US Department of Energy, Office of Nuclear Energy Molten Salt Chemistry Workshop*, 2017.

(2) OECD Nuclear Energy Agency on behalf of *the Generation IV International Forum, Technology Roadmap Update for Generation IV Nuclear Energy Systems*, 2014.

(3) Cordfunke, E. H. P.; Barczewski, O. The thermochemical properties of the system uranium—oxygen—chlorine. *Thermochim. Acta* **1984**, 74, 235−245.

(4) Oman, S.; Picton, G.; Ruckman, J. C. Uranium Oxides Formed in Air and Water in the Temperature Range 200−375°C. *Oxid. Met.* **1969**, 1, 199−207.

(5) Allen, G. C.; Tempest, P. A.; Garner, C. D.; Ross, I.; Jones, D. J. EXAFS: A New Approach to the Structure of Uranium Oxides. *J. Phys. Chem. B* **1985**, 89 (8), 1334−1336.

(6) Hoekstra, H. R.; Siegel, S. The Uranium-Oxygen System: U_3O_8-UO_3. *J. Inorg. Nucl. Chem.* **1961**, 18, 154−165.

(7) Martynova, N. S.; Vasil'kova, I. V.; Susarev, M. P. Thermographic Investigation of UO_2, UCl, AND KCl Ternary and Binary Systems. *Sov. At. Energy* **1965**, 18, 777−783.

(8) Smirnov, Mv.; Komarov, V. E.; Koryushin, A. P. Decomposition of Uranyl Chloride and With Uranium Dioxide in Molten NaCl. *Sov. At. Energy* **1967**, 22, 34−37.

(9) Wilkerson, M. P.; Burns, C. J.; Paine, R. T.; Scott, B. L. Synthesis and crystal structure of $UO_2Cl_2(THF)_3$: A simple preparation of an anhydrous uranyl reagent. *Inorg. Chem.* **1999**, 38, 4156−4158.

(10) Servaes, K.; Hennig, C.; van Deun, R.; Görller-Walrand, C. Structure of $[UO_2Cl_4]^{2-}$ in acetonitrile. *Inorg. Chem.* **2005**, 44, 7705−7707.

(11) Bean, A. C.; Xu, Y.; Danis, J. A.; Albrecht-Schmitt, T. E.; Scott, B. L.; Runde, W. Aqueous reactions of U(VI) at high chloride concentrations: Syntheses and structures of new uranyl chloride polymers. *Inorg. Chem.* **2002**, 41, 6775−6779.

(12) Hennig, C.; Tutschku, J.; Rossberg, A.; Bernhard, G.; Scheinost, A. C. Comparative EXAFS investigation of uranium(VI) and -(IV) aquo chloro complexes in solution using a newly developed spectroelectrochemical cell. *Inorg. Chem.* **2005**, 44, 6655−6661.

(13) Lee, C. A.; van Veelen, A.; Morris, K.; Mosselmans, J. F. W.; Wogelius, R. A.; Burton, N. A. Uranium (VI) adsorbate structures on portlandite $[Ca(OH)_2]$ type surfaces determined by computational modelling and X-ray absorption spectroscopy. *Minerals* **2021**, 11, 1241.

(14) Uehara, A.; Fujii, T.; Yamana, H.; Okamoto, Y. An in-situ X-ray absorption spectroelectrochemical study of the electroreduction of uranium ions in HCl, HNO_3, and Na_2CO_3 solutions. *Radiochim. Acta* **2016**, 104, 1−9.

(15) Okamoto, Y.; Akabori, M.; Itoh, A.; Ogawa, T. X-ray absorption study of molten uranium chloride system. *J. Nucl. Sci. Technol.* **2002**, 39, 638−641.

(16) Li, X.; Song, J.; Shi, S.; et al. Dynamic fluctuation of U^{3+} coordination structure in the molten LiCl-KCl eutectic via first principles molecular dynamics simulations. *J. Phys. Chem. A* **2017**, 121, 571−578.

(17) Wang, S.; Xiao, S.; Hu, W.; Deng, H. Effect of MCl_3 (M=La, U or Sc) component on the local structures and transport properties of LiCl−KCl−MCl_3 eutectic: A molecular dynamics study. *Electrochim. Acta* **2019**, 306, 366−376.

(18) Dai, J. X.; Zhang, W.; Ren, C. L.; Han, H.; Guo, X. J.; Li, Q. N. Molecular dynamics investigation on the local structures and transport properties of uranium ion in LiCl-KCl molten salt. *J. Nucl. Mater.* **2018**, 511, 75−82.

(19) Song, J.; Shi, S.; Li, X.; Yan, L. First-principles molecular dynamics modeling of UCl_3 in LiCl-KCl eutectic. *J. Mol. Liq.* **2017**, 234, 279−286.

(20) Kosog, B.; la Pierre, H. S.; Denecke, M. A.; Heinemann, F. W.; Meyer, K. Oxidation state delineation via U L III-edge XANES in a series of isostructural uranium coordination complexes. *Inorg. Chem.* **2012**, 51, 7940−7944.

(21) Liu, Y. L.; Yuan, L. Y.; Zheng, L. R.; et al. Confirmation and elimination of cyclic electrolysis of uranium ions in molten salts. *Electrochem. Commun.* **2019**, 103, 55−60.

(22) Yingling, J. A.; Schorne-Pinto, J.; Aziziha, M.; et al. Thermodynamic measurements and assessments for LiCl-NaCl-KCl-UCl_3 systems. *J. Chem. Thermodyn.* **2023**, 179, No. 106974.

(23) Kiss, A. M.; Harris, W. M.; Nakajo, A.; et al. In Situ Heater Design for Nanoscale Synchrotron-Based Full-Field Transmission X-Ray Microscopy. *Microsc. Microanal.* **2015**, 21, 290−297.

(24) Lynch, T. J.; Birkner, N. R.; Christian, M. S.; et al. In Situ Determination of Speciation and Local Structure of NaCl-$SrCl_2$ and LiF-ZrF_4 Molten Salts. *J. Phys. Chem. B* **2022**, 126, 1539−1550.

(25) Ravel, B.; Newville, M. ATHENA, ARTEMIS, HEPHAESTUS: Data analysis for X-ray absorption spectroscopy using IFEFFIT. *J. Synchrotron Radiat.* **2005**, 12, 537−541.

(26) Lynch, T. J. In-Situ High Temperature Measurement and Validation of Molten Salt Properties, M.S. Thesis. M.S. Thesis, University of Connecticut, 2022.

(27) Tamasi, A. L.; Boland, K. S.; Czerwinski, K.; et al. Oxidation and hydration of U_3O_8 materials following controlled exposure to temperature and humidity. *Anal. Chem.* **2015**, 87, 4210−4217.

(28) Debets, P. C. The structures of uranyl chloride and its hydrates. *Acta Crystallogr., Sect. B: Struct. Crystallogr. Cryst. Chem.* **1968**, 24, 400−402.

(29) Taylor, J. C.; Wilson, P. W. The Structure of Uranium(III) Trichloride by Neutron-Diffraction Profile Analysis. *Acta Cryst.* **1974**, B30, 2803−2805.

(30) Loopstra, B. O. The structure of B-U3O8. *Acta Cryst.* **1970**, B26, 656−657.

(31) Wasserstein, B. Cube-edges of Uraninites as a criterion of age. *Nature* **1951**, 168, 380.

(32) Nazarchuk, E. V.; Siidra, O. I.; Krivovichev, S.V. Crystal Chemistry of Uranyl Halides Containing Mixed $(UO_2)(X_mO_n)_5$ Bipyramids (X = Cl, Br): Synthesis and Crystal Structure of $Cs_2(UO_2)(NO_3)Cl_3$. *Z. Naturforsch. B* **2011**, 66, 142−147.

(33) Tuffy, B. W.; Birkner, N. R.; Schorne-Pinto, J.; Davis, R. C.; Mofrad, A. M.; Dixon, C. M.; Aziziha, M.; Christian, M. S.; Lynch, T. J.; Bartlett, M. T.; Besmann, T. M.; Brinkman, K. S.; Chiu, W. K. S.

Formation of β-U₃O₈ from UCl₃ Salt Compositions Under Oxygen Exposure. *Manuscript submitted*, **2023**.

(34) Danis, J. A.; Lin, M. R.; Scott, B. L.; Eichhorn, B. W.; Runde, W. H. Coordination trends in alkali metal crown ether uranyl halide complexes: The series [A(crown)]₂[UO₂X₄] where A = Li, Na, K and X = Cl, Br. *Inorg. Chem.* **2001**, *40*, 3389−3394.

(35) Jones, L. H. Systematics in the vibrational spectra of uranyl complexes. *Spectrochim. Acta* **1958**, *10*, 395−403.

(36) Dargent, M.; Dubessy, J.; Truche, L.; Bazarkina, E. F.; Nguyen-Trung, C.; Robert, P. Experimental study of uranyl(VI) chloride complex formation in acidic LiCl aqueous solutions under hydrothermal conditions (T = 21 °C−350 °C, Psat) using Raman spectroscopy. *Eur. J. Mineral.* **2013**, *25*, 765−775.

(37) Polovov, I. B.; Volkovich, V. A.; Charnock, J. M.; et al. In situ spectroscopy and spectroelectrochemistry of uranium in high-temperature alkali chloride molten salts. *Inorg. Chem.* **2008**, *47*, 7474−7482.

(38) Nguyen-Trung, C.; Begun, G. M.; Palmer, D. A. Aqueous Uranium Complexes. 2. Raman Spectroscopic Study of the Complex Formation of the Dioxouranium(VI) Ion with a Variety of Inorganic and Organic Ligands. *Inorg. Chem* **1992**, *31*, 5280−5287.

(39) Fujii, T.; Uda, T.; Iwadate, Y.; Nagai, T.; Uehara, A.; Yamana, H. Raman spectroscopic study of uranyl complex in alkali chloride melts. *J. Nucl. Mater.* **2013**, *440*, 575−579.